Linking dielectric dispersion and age in brain tissues via water content-based Electric Properties Tomography

NeuroImage 322 (2025) 121559

Contents lists available at ScienceDirect

NeuroImage

journal homepage: www.elsevier.com/locate/ynimg

Linking dielectric dispersion and age in brain tissues via water content-based Electric Properties Tomography

Sébastien Marmin [a], Alessandro Arduino [b], Matteo Cencini [c], Marta Lancione [c], Laura Biagi [c], Michela Tosetti [c,*], Luca Zilberti [b]

[a] Laboratoire national de métrologie et d'essais, 1 Rue Gaston Boissier, 75015 Paris, France
[b] Istituto Nazionale di Ricerca Metrologica, Strada delle Cacce 91, 10135 Turin, Italy
[c] IRCCS Stella Maris Foundation, Viale del Tirreno 331-341 56128 Pisa, Italy

ARTICLE INFO

Dataset link: https://github.com/SebastienMarmin/brain-water-content-ept-values

Keywords:
Electric properties tomography (EPT)
Brain development
Conductivity maps
Dielectric dispersion

ABSTRACT

Popular dielectric dispersion models of biological tissues, which describe dielectric properties as a function of frequency, do not account for age-related variations. In particular, existing databases have limited validity in pediatric populations. In this work, we applied water content-based Electric Properties Tomography in vivo to healthy subjects across the lifespan to incorporate age-related information into dielectric dispersion models of white and grey matter. Water content, derived from magnetic resonance fingerprinting-based T_1 mapping, was modelled as a function of age. The age-water relationships was then integrated with Cole-Cole dispersion via water-dependent permittivity and conductivity equations. The resulting model allows obtaining age-specific conductivity and permittivity of brain tissues at frequencies higher than 50 MHz. In addition, it provides confidence intervals accounting for both intra-subject and inter-subject variability. In terms of applications for brain studies, this model enables age-specific electromagnetic simulations for pediatric subjects and evaluations on the safety of electromagnetic exposure in developing brains. An open code is freely available online to compute electrical properties and their uncertainties as a function of frequency and age.

1. Introduction

Accurate estimations of the dielectric property values are essential for simulating the interaction between electromagnetic fields and biological tissues and establishing their possible adoption as physical biomarkers. After the publication of the results of Gabriel's group in 1996 (Gabriel et al., 1996a,b,c), the 4th order Cole-Cole dispersion model became the gold standard to obtain reference values of the dielectric properties of human biological tissues. Such model, including the identified optimal parameters (obtained by fitting data measured on samples mostly coming from freshly killed ovine and porcine, and some ex-vivo human tissues), is adopted within popular databases of tissue properties, like the IT'IS Foundation database (Baumgartner et al., 2025). The model relates the dielectric property values to the frequency of the electromagnetic radiation to which the tissue is exposed, but it does not account for age-related effects. The variation with age of dielectric properties of mammalians' tissues has been documented extensively, with special focus on the brain, starting from the 1980s (Thurai et al., 1984, 1985; Peyman et al., 2001, 2007). The drift of such properties has been associated with a corresponding drift of tissues' water content, which tends to decrease with age, and make the existing databases not reliable in providing an estimate of tissues dielectric properties in children. It is then essential to investigate the proper correction of the dispersion models according to age, in order to avoid the risk of incorrect safety estimations, biased simulation models, or blurred comparisons of dielectric properties in pediatric populations (Gabriel and Peyman, 2018; Wang et al., 2006; Peyman et al., 2009; Malik et al., 2021, 2022).

In high water content tissues, such as the brain, it can be assumed that the dielectric properties are mainly modulated by water content (Michel et al., 2017). Hence, age-specific dispersion models can be produced by measuring the variation of water content in the brain across the lifespan. To this aim, we reconstructed water content (w) maps from T_1 maps (Fatouros and Marmarou, 1999) acquired using Magnetic Resonance Imaging (MRI) on healthy subjects of different ages and performed water content Electric Properties Tomography (wEPT) (Michel et al., 2017; Cencini et al., 2024; Mandija et al., 2023). Exploiting the relationships between w, wEPT and age, we aim to provide an age-specific estimate of the dielectric properties of grey and white matter for frequencies from 50 MHz to 700 MHz. After presenting

* Correspondence to: IRCCS Stella Maris Foundation, Pisa, Italy.
E-mail address: michela.tosetti@fsm.unipi.it (M. Tosetti).

https://doi.org/10.1016/j.neuroimage.2025.121559
Received 15 June 2025; Received in revised form 21 October 2025; Accepted 24 October 2025
Available online 30 October 2025

the experiments performed to collect the input data and the data processing, we describe an analysis in two steps: first, we establish a relation between water content and age; then, we formulate the electric properties as a function of water content. The age-specific dielectric model resulting from chaining of these two relations is discussed in terms of uncertainty quantification.

2. Methods

2.1. Data acquisition and processing

Data from $n = 27$ healthy subjects (0.8–55 years old, 16 males/11 females) were acquired using a 1.5 T GE HealthCare HDxt scanner using a quadrature-mode body coil for transmission and an 8-channel head coil for reception. Adult subjects volunteered to participate in the study and gave their written informed consent. Pediatric subjects were retrospectively selected from a cohort of patients that underwent a clinical MR scan that was followed by the acquisition of sequences for research purposes. In particular, we identified subjects with minor clinical indications (e.g., headache, paroxysmal or ictal episode) and that had a normal MRI examination. Their parents gave their written informed consent. The study was approved by the local ethical committee. Subsets of this dataset were previously analysed in Cencini et al. (2024) and Lancione et al. (2024).

Each subject underwent a 3D Steady State Free Precession MR Fingerprinting (MRF) acquisition consisting of a variable flip angle scheme preceded by an adiabatic inversion pulse, with fixed TE (0.5 ms) and TR (8.5 ms) for a total scan time of 7 minutes. k-Space sampling was performed using a 3D spiral projection trajectory (FOV = 225 mm × 225 mm × 225 mm; voxel size = 1.125 mm × 1.125 mm × 1.125 mm) (Gómez et al., 2020). Image reconstruction was performed offline and consisted of a zero-filled backprojection onto a low-rank subspace basis determined by Singular Value Decomposition (McGivney et al., 2014) of a database of simulated MRF signals obtained using Extended Phase Graphs (Weigel, 2015). Data were combined using ESPIRiT approach (Uecker et al., 2014) and used to estimate quantitative T_1, T_2 and M_0 maps based on a fully-connected neural network (Gómez et al., 2020), also trained using simulated MRF data.

A synthetic T_1-weighted image $T_{1,w}^{\text{synth}}$ was derived from the MRF T_1 map simulating the signal of an inversion recovery sequence as $T_{1,w}^{\text{synth}} = 1 - 2e^{-\text{TI}/T_1}$, using TI = 220 ms as the inversion time. The $T_{1,w}^{\text{synth}}$ image was skull stripped using hd-bet (Isensee et al., 2019) and tissue class segmentation was performed using FSL-FAST (Zhang et al., 2001). The grey matter (GM) and white matter (WM) probabilistic masks were binarized by applying a threshold of 0.7.

MRF-derived T_1 maps were used to perform a voxel-wise estimation of water content according to the following equation:

$$w = \frac{T_1}{AT_1 + B} \tag{1}$$

where A and B are two constants fitted to experimental data with the least square method. The water content values used for the calibration correspond to the reference values in adult white matter (69.49% ± 2.55%), grey matter (81.55% ± 4.36%) and cerebrospinal fluid (99.37% ± 2.38%) provided by the IT'IS Foundation database (Baumgartner et al., 2025), while the T_1 values are the median observed in our adult data. Fitting was performed by nonlinear least squares to obtain point estimates of the parameters A and B. Because both the calibration water content values and the measured T_1 medians have uncertainty, we estimated the uncertainty and the joint sampling distribution of (A, B) with a parametric Monte Carlo procedure (See Section 2.4 for details).

Finally, the median water content and the 25th and 75th percentiles were measured within the GM and WM masks for each subject.

2.2. Water content as a function of age

To deduce the dependence on age of the electric properties at frequencies in the range from 50 MHz to 700 MHz, we first looked for the trend of the water content w with respect to the age. For each subject and each tissue type, the median and the percentiles of the w values were used to fit a heteroscedastic statistical model, using an exponential decay function in both WM and GM

$$w(t; a, \alpha, w_\infty) = ae^{-t/\alpha} + w_\infty, \tag{2}$$

where t is the subject age, whereas the coefficient a, the time constant α and the asymptotic value w_∞ are fitting parameters. The same type of exponential decay model was used in Gräfe et al. (2021) for T_1 values.

The residual variance of the fitting, covering both the intra-subject and inter-subject variability observed in w measurements, was estimated by parametric bootstrapping, where each water content estimate follows a normal distribution with age-independent variances (see Section 2.4 for details).

2.3. Electric properties as a function of water content

According to previous works (Michel et al., 2017; Cencini et al., 2024), the conductivity σ and the relative permittivity ε_r of brain tissues can be expressed as

$$\sigma = c_1 + c_2 e^{c_3 w}, \qquad \varepsilon_r = p_1 w^2 + p_2 w + p_3 \tag{3}$$

where the c_i and p_i coefficients must be calibrated at each frequency of interest. Three reference points were used for the calibration of the c_i coefficients: $(w_{\text{ref}}^{\text{WM}}, \sigma^{\text{WM}})$, $(w_{\text{ref}}^{\text{GM}}, \sigma^{\text{GM}})$ and $(w_{\text{ref}}^{\text{CSF}}, \sigma^{\text{CSF}})$. The conductivity reference values of WM, GM, and cerebrospinal fluid (CSF) (denoted by σ^{WM}, σ^{GM}, σ^{CSF}) were obtained by applying the 4th order Cole-Cole model with the parameters extracted from the IT'IS Foundation database (Baumgartner et al., 2025). Calibration water content values were chosen equal to those used to fit Eq. (1), as provided by the IT'IS Foundation database (Baumgartner et al., 2025). An analogous procedure was followed with relative permittivity in place of electric conductivity for the calibration of the p_i coefficients. The resulting curves using nominal values are shown in Fig. 1. We notice that, for permittivity, the trend with the water content may be non-monotonic, depending on the considered frequency. The uncertainty of the calibration water content values is provided by the database, whereas the uncertainty in the electrical property values is assumed equal to 10% of each nominal value (Gabriel et al., 1996b).

Following this procedure, age-specific values of conductivity and permittivity in WM and GM were finally obtained by substituting Eq. (2) into Eq. (3). The uncertainty is propagated through this model with a Monte Carlo approach detailed in the next section.

2.4. Uncertainty propagation

The uncertainty quantification combines intra-subject spatial dispersion, inter-subject variability for subjects with similar age and measurement error variability in water content estimation with Monte Carlo propagation through dielectric property models.

The standard uncertainty in water content u_w derives from parametric bootstrapping of water content data (see Eq. (2)). Multiple repetitions of nonlinear least-squares fitting were computed from perturbed water content data. The perturbation consists in additive uniform noise with the length of the distribution interval given by the 5th and 95th percentiles of the intra-subject spatial dispersion including the calibration variability of Eq. (1). Specifically, we performed $N = 10\,000$ Monte Carlo replications. In each replication we: (i) sampled each calibration water content value from a uniform distribution centred on the reference value and spanning the uncertainty range (Baumgartner et al., 2025); (ii) sampled each T_1 calibration point from a normal distribution with mean equal to the observed median T_1 in adults and

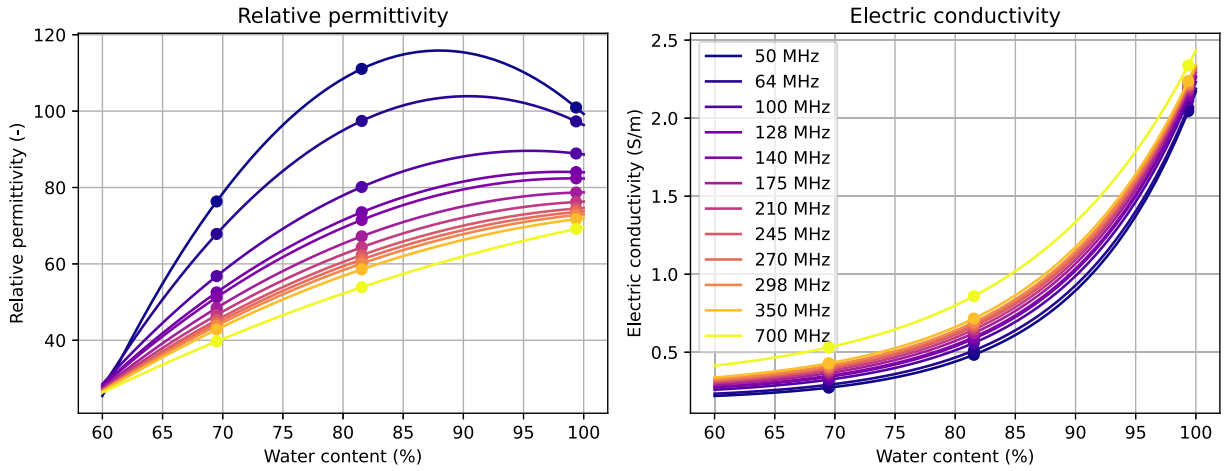

Fig. 1. Relative permittivity (left) and electrical conductivity (right) plotted as a function of the water content, for different frequencies. The dots indicate the reference values used to deduce the fitting parameters required in Eq. (3).

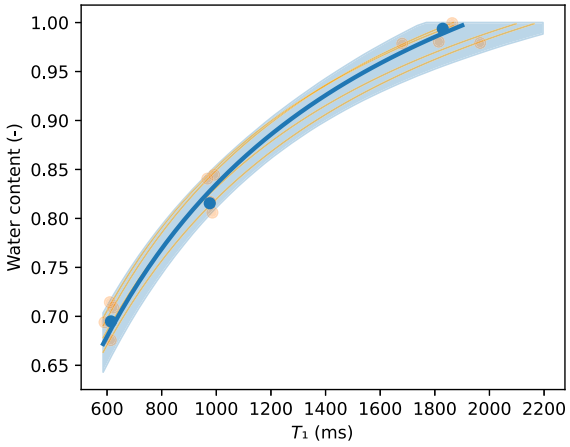

Fig. 2. Calibration of the water content versus T_1 (blue line) from least square fits of the values reported in the IT'IS Foundation database (Baumgartner et al., 2025) and the corresponding median T_1 values measured in our adult cohort (blue dots). Some examples of curves from Monte Carlo sample pairs of calibration parameters (A, B) are also displayed (orange lines and dots). The uncertainty envelope corresponds to the 95% Monte Carlo confidence interval. (For interpretation of the references to colour in this figure legend, the reader is referred to the web version of this article.)

standard deviation equal to the estimated standard uncertainty of that median; (iii) fit the least-square model to obtain one sample pair (A, B). The N fitted pairs provide an empirical joint distribution for (A, B), from which we report percentile-based uncertainty intervals and the empirical correlation between A and B (see Section 3). To visually demonstrate the calibration robustness, Fig. 2 shows the variability of the three calibration points, the fitted curve from the nominal points, and four Monte Carlo fitted curves. This figure highlights that the w-T_1 relationship is stable within the reported calibration uncertainty.

The errors between the ith bootstrap prediction at the jth individual are supposed centred, independent and identically distributed, leading to the estimate

$$u_w = \sqrt{\frac{1}{N(n-1)} \sum_{i=1}^{N} \sum_{j=1}^{n} (w_{ij} - \bar{w}_j)^2}, \tag{4}$$

with $\bar{w}_j$ the average of bootstraps predictions over each of the n individuals. For the two tissues, we obtain $u_w^{\mathrm{WM}} = 0.019$ and $u_w^{\mathrm{GM}} = 0.022$.

Another Monte Carlo propagation is needed due to the strong non-linearity observed for the electrical properties with respect to water content (see Eq. (3) and Fig. 1), taking into account the uncertainty in water content u_w, and the uncertainties of the calibration points $(w_{\mathrm{ref}}^{\mathrm{WM}}, \sigma^{\mathrm{WM}})$, $(w_{\mathrm{ref}}^{\mathrm{GM}}, \sigma^{\mathrm{GM}})$ and $(w_{\mathrm{ref}}^{\mathrm{CSF}}, \sigma^{\mathrm{CSF}})$. The uncertainties in water content calibration points are provided by the IT'IS Foundation database (Baumgartner et al., 2025), whereas we assume a relative uncertainty of 10% in the electrical properties reference values. The latter uncertainty is pragmatic choice for the frequency range used in this work (50 MHz to 700 MHz), and originates from the fact that, for the three considered tissues, the IT'IS Foundation database refers to the data collected by Gabriel's group (Gabriel et al., 1996b), which, according to the authors, exhibited a spread of values of ±5% to 10% above 100 MHz. The conservative 10% uncertainty is intended here as a compromise with lower frequencies (near 50 MHz) where Gabriel reports larger spreads (±15% and possibly 25% at the very lowest end of the frequency scale). The uncertainty propagation is performed by Monte Carlo simulation assuming a normal distribution (truncated at $w > 1$) of the water content reference values and a uniform distribution of the electrical properties reference values.

This two-stage process follows the Guide to the Expression of Uncertainty in Measurement (Joint committee for guides in metrology (JCGM), 2008a,b).

3. Results

Water content maps and dielectric property maps were successfully reconstructed for all subjects. The calibration values of Eq. (1), obtained with the fitting of our experimental T_1 data to the reference water content values (Baumgartner et al., 2025), are $A = 0.7866$ and $B = 411$ ms. Representative maps of electric conductivity and relative permittivity acquired at 1.5 T (64 MHz) are displayed in Fig. 3 for subjects of different ages. It can be observed that both σ and ε_r tend to decrease with age.

The median, the 25th and the 75th percentiles of T_1 and water content values in GM and WM are displayed with respect to subject age in Fig. 4, together with the fitted curve for w. The parameter of the fit are reported in Table 1 and indicate similar water content decline rate in WM ($\alpha =$ 3.3 years) and GM ($\alpha =$ 3.8 years).

The curves of the conductivity and permittivity as a function of water content are shown in Fig. 1. The fitted curves were visually inspected against the measured data (Fig. 4), showing excellent agreement across the age range (0.8–55 years). The residuals exhibited no systematic trends, confirming the exponential decay model (Figure ??). The uncertainty of σ and ε_r with respect to w (assuming an uncertainty

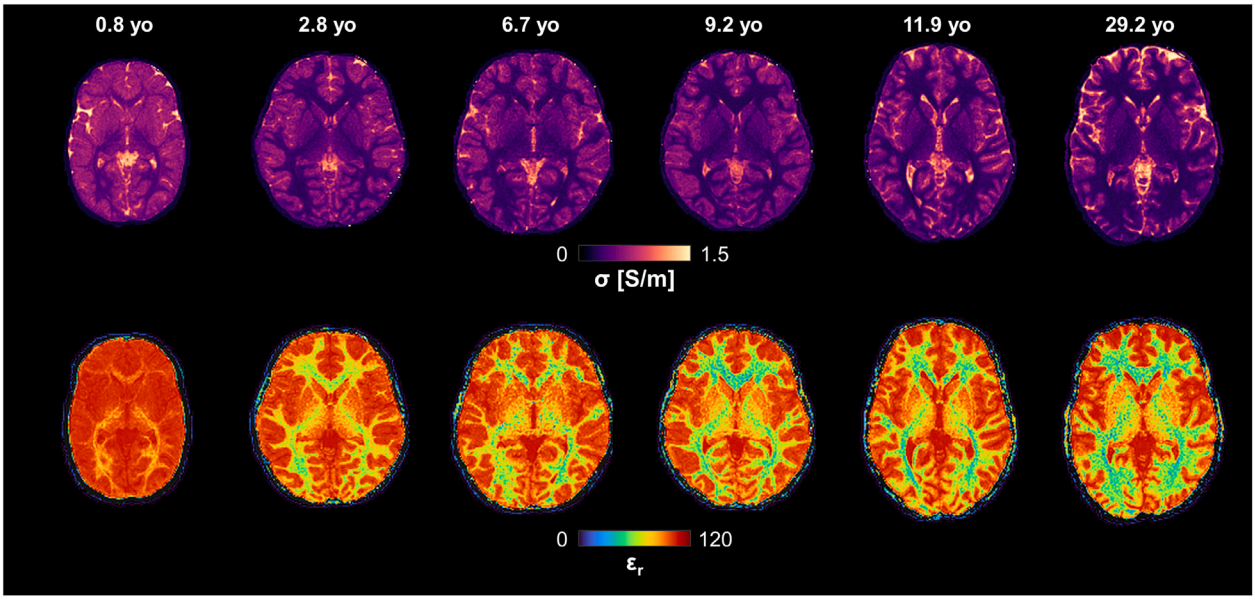

Fig. 3. Electric conductivity (top) and relative permittivity (bottom) maps measured at 1.5 T (64 MHz) for six representative subjects of different ages. The reduction of both conductivity and permittivity with age can be observed. The colorbars use linear scales. (For interpretation of the references to colour in this figure legend, the reader is referred to the web version of this article.)

Table 1
Indications of the water content exponential decays with respect to age estimated using the model described in Eq. (2).

	White matter	Grey matter
Coefficient a	0.16985	0.097671
Exponential time constant α (years)	3.3119	3.7510
Adult asymptotic value w_∞	0.68670	0.82920

in the water content equal to 0.019) can be visualized in Fig. 5. Age dependence enters through $w(t)$ trajectories (Eq. (2)), with final uncertainties visualized in Fig. 6.

The EP values obtained at various age are reported in Table 2.

The estimated conductivity and permittivity according to subject age and frequency are displayed in Figs. 7 and 8. Frequency-age surfaces for σ and ε_r show nonlinear declines, steepest before 10 years old and at lower frequencies. Fig. 6 shows the trends of relative permittivity and electrical conductivity in WM and GM as a function of age at different frequencies (including the proton Larmor frequencies at 1.5 T, 3 T and 7 T), with the evaluation of uncertainty.

4. Discussion

This work shows how to get age-specific values of the dielectric parameters of WM and GM at the frequency of interest, along with an uncertainty accounting for the intra-subject and inter-subject variability.

Our work relies on T_1 values measured using MRF, which show reasonable agreement with values in the literature for adult subjects (Cho et al., 1997). For children aged 2–12 years, our observed T_1 decrease with age aligns with trends reported at 3 T by Gräfe et al. (2021). For instance in WM, at age 3, our decrease of −52 ms/year compares closely with their occipital (−52 ms/year) and frontal WM values (−59 ms/year). Similarly, at age 7, our rate of −13 ms/year corresponds to their measurements (−14 and −15 ms/year). Furthermore, estimating a constant slope between ages 2 and 17, Romascano et al. (2024) finds a decrease in T_1 in white matter of −5.3 ms/year. We obtain a comparable average decrease, −4.9 ms/year, over the same range.

One key aspect of the adopted EPT method is the use of the water content, which, being invariant, allows getting data for frequencies other than the Larmor frequency of the MR scans used to acquire the data. This generalizes currently available databases of dielectric properties, without requiring age-specific MR scans at every frequency. An essential feature of this outcome is a frequency-dependent conductivity and permittivity distribution that may expand the ability to provide diagnostic information.

The obtained results may find application in two different contexts. First, they can be used to perform numerical simulations describing human exposure to electromagnetic fields, taking into account age (Peyman et al., 2009; Malik et al., 2021, 2022) and statistical variability (Bottauscio et al., 2024). Besides safety assessment in numerical dosimetry applications of non-ionizing radiation protection (Fiocchi et al., 2013; Chiaramello et al., 2018), such simulations could benefit the optimization of radiofrequency coil designs for pediatric MRI (Gilbert et al., 2023).

The results can also be used to get age-specific physiological ranges of conductivity and permittivity, in case such parameters are to be used as diagnostic biomarkers (Park et al., 2019; Lesbats et al., 2021). As age may act as a confounding factor (w may be different from normative values due to a pathologies, but also due to the developmental age), we underline that the knowledge of physiological ranges, instead of single values, is a first essential requirement to allow quantifying the risk of false positive diagnostic outcomes, whenever a subject exhibits brain dielectric properties that deviates from normal range values. While the diagnostic applicability of EPT in the brain has been documented for an unspecific age (Zhang et al., 2014; Liu et al., 2017), correcting the normal range values of electrical properties according to the subject age is a key step in understanding the applicability in pediatric contexts.

In both applications mentioned above, the identification of the voxels belonging to white and grey matter plays a key role. This is evident for electromagnetic dosimetry, where the properties provided by the age-specific dispersion model must be applied to the corresponding tissue. The correct identification of the tissue (i.e., the segmentation process) is also crucial for diagnostic purposes in the presence of pathologies that influence the value of the water content, to compare the dielectric properties measured with the normal ranges of corresponding healthy tissues.

Methodological limitations include the use of empirical models to derive σ and ε_r from T_1 and the reliance on three calibration points from literature for Eq. (3). However, we propagated their uncertainties

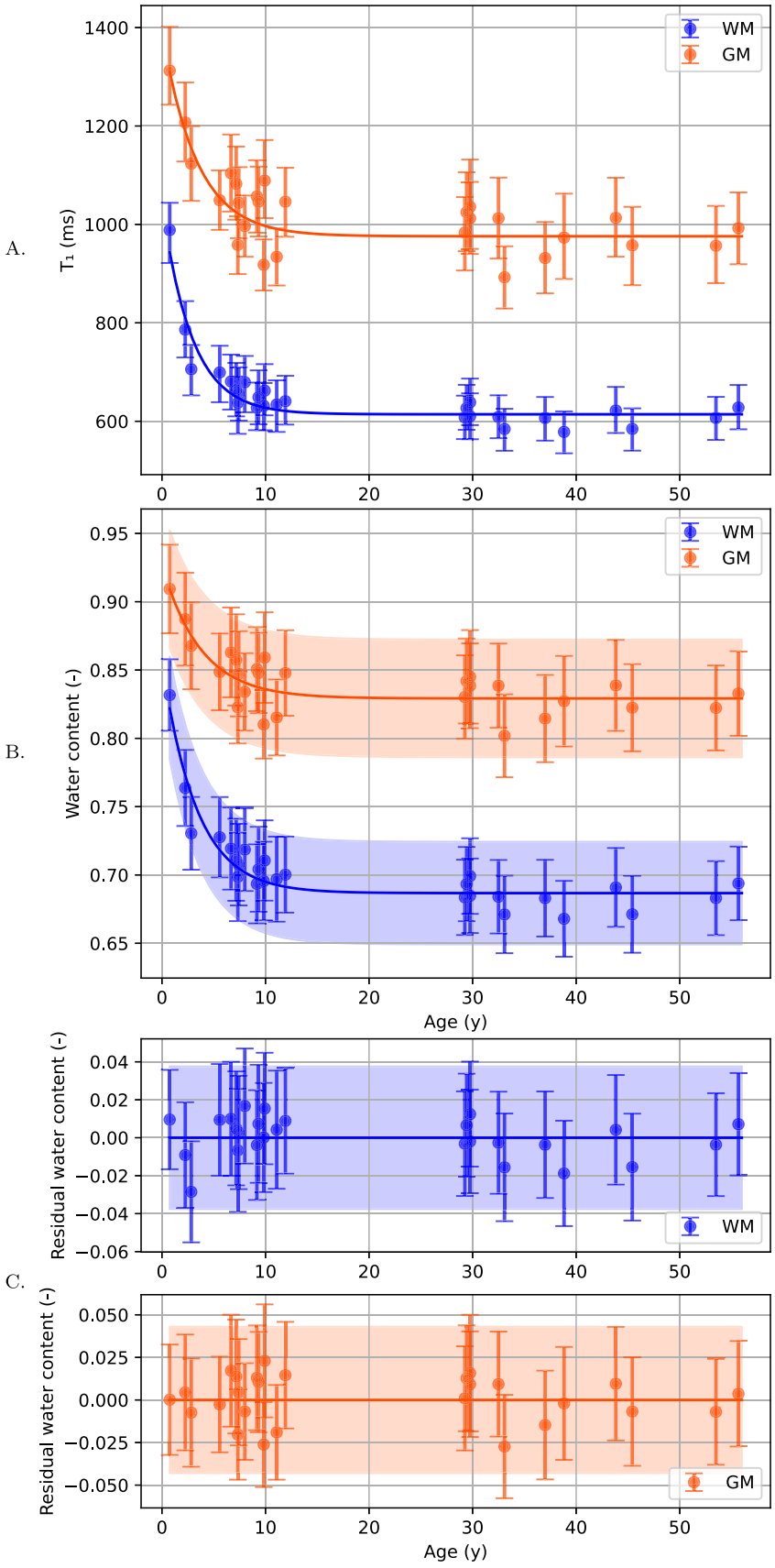

Fig. 4. T_1 (A), water content (B) values in the brain of the subjects, including water content calibration variability, as a function of their age. The circles indicate the median values; whiskers range from the 25th to the 75th percentiles. For water content, regression curves are reported as solid lines and the shaded bands represent the prediction intervals (water content uncertainty with coverage factor $k = 2$). The panel C shows water content residual values.

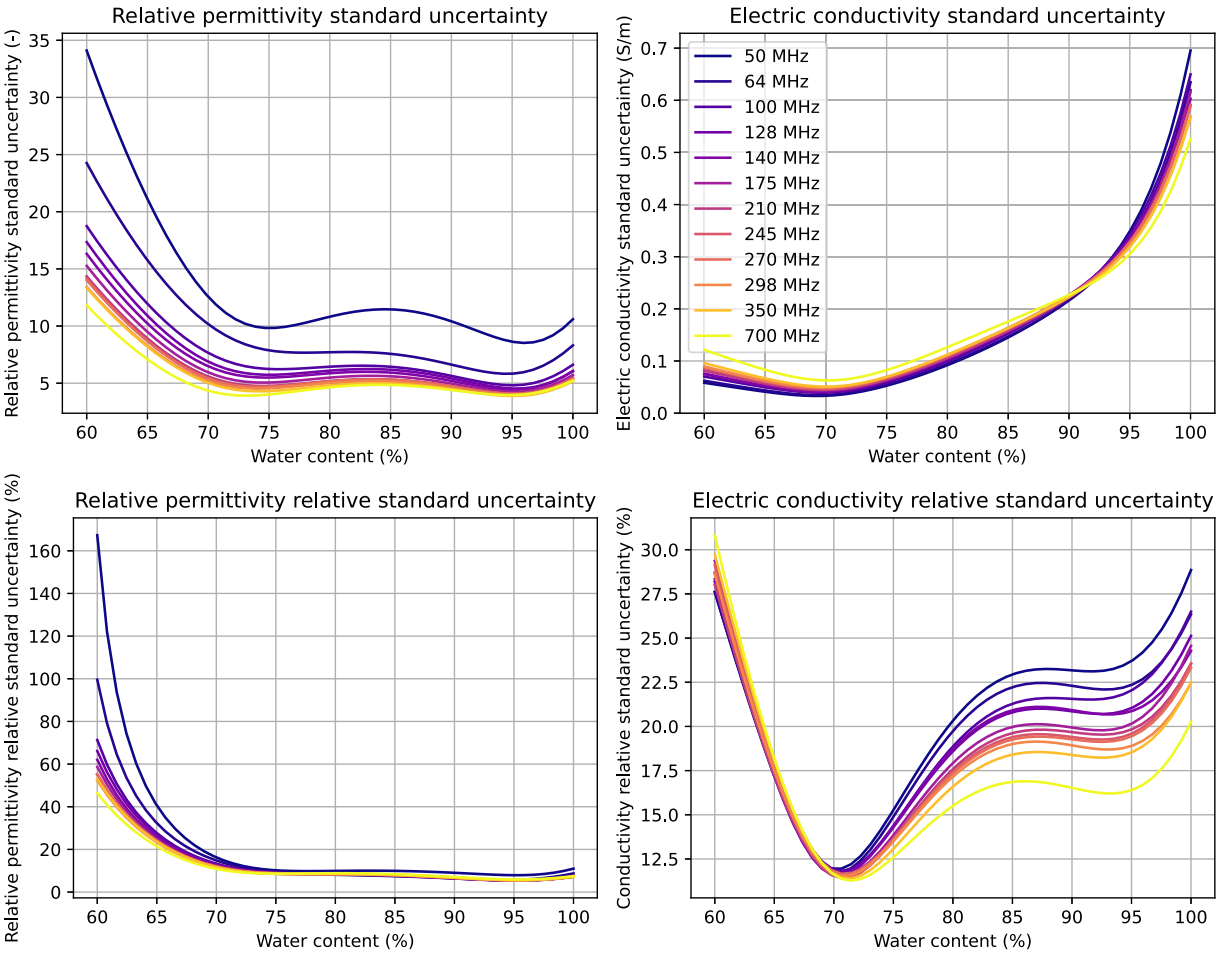

Fig. 5. Absolute (top) and relative (bottom) uncertainty of relative permittivity (left) and electrical conductivity (right) plotted as a function of the water content, for different frequencies.

Table 2
Conductivity $\sigma(w(t))$ (S/m) and relative permittivity $\varepsilon_r(w(t))$ (Section 2.3, Fig. 6), for different ages, frequencies and tissues, with uncertainties with coverage factor $k = 2$ (Section 2.4).

Age (years)	0.8	3	10	55
64 MHz - 1.5 T				
WM	σ = 0.55 ± 0.21	σ = 0.37 ± 0.11	σ = 0.291 ± 0.064	σ = 0.282 ± 0.065
	ε_r = 99 ± 14	ε_r = 86 ± 14	ε_r = 67 ± 19	ε_r = 64 ± 21
GM	σ = 1.05 ± 0.45	σ = 0.78 ± 0.34	σ = 0.60 ± 0.25	σ = 0.57 ± 0.23
	ε_r = 104 ± 12	ε_r = 103 ± 13	ε_r = 100 ± 14	ε_r = 100 ± 14
128 MHz - 3 T				
WM	σ = 0.62 ± 0.23	σ = 0.44 ± 0.12	σ = 0.342 ± 0.074	σ = 0.332 ± 0.074
	ε_r = 75 ± 12	ε_r = 64 ± 11	ε_r = 52 ± 13	ε_r = 50 ± 14
GM	σ = 1.14 ± 0.46	σ = 0.87 ± 0.36	σ = 0.68 ± 0.27	σ = 0.65 ± 0.25
	ε_r = 82.3 ± 9.9	ε_r = 80 ± 11	ε_r = 76 ± 12	ε_r = 75 ± 12
298 MHz - 7 T				
WM	σ = 0.73 ± 0.25	σ = 0.52 ± 0.13	σ = 0.411 ± 0.089	σ = 0.399 ± 0.091
	ε_r = 61.0 ± 9.5	ε_r = 52.6 ± 8.3	ε_r = 43 ± 10	ε_r = 42 ± 11
GM	σ = 1.26 ± 0.47	σ = 0.99 ± 0.37	σ = 0.79 ± 0.29	σ = 0.76 ± 0.28
	ε_r = 68.8 ± 8.6	ε_r = 66.0 ± 9.5	ε_r = 62.5 ± 9.8	ε_r = 61.8 ± 9.7
700 MHz				
WM	σ = 0.90 ± 0.27	σ = 0.67 ± 0.16	σ = 0.53 ± 0.12	σ = 0.51 ± 0.12
	ε_r = 54.8 ± 8.8	ε_r = 47.2 ± 7.4	ε_r = 39.4 ± 8.4	ε_r = 38.3 ± 9.0
GM	σ = 1.44 ± 0.47	σ = 1.17 ± 0.39	σ = 0.97 ± 0.31	σ = 0.93 ± 0.30
	ε_r = 63.1 ± 8.4	ε_r = 59.9 ± 9.1	ε_r = 56.2 ± 9.1	ε_r = 55.5 ± 9.1

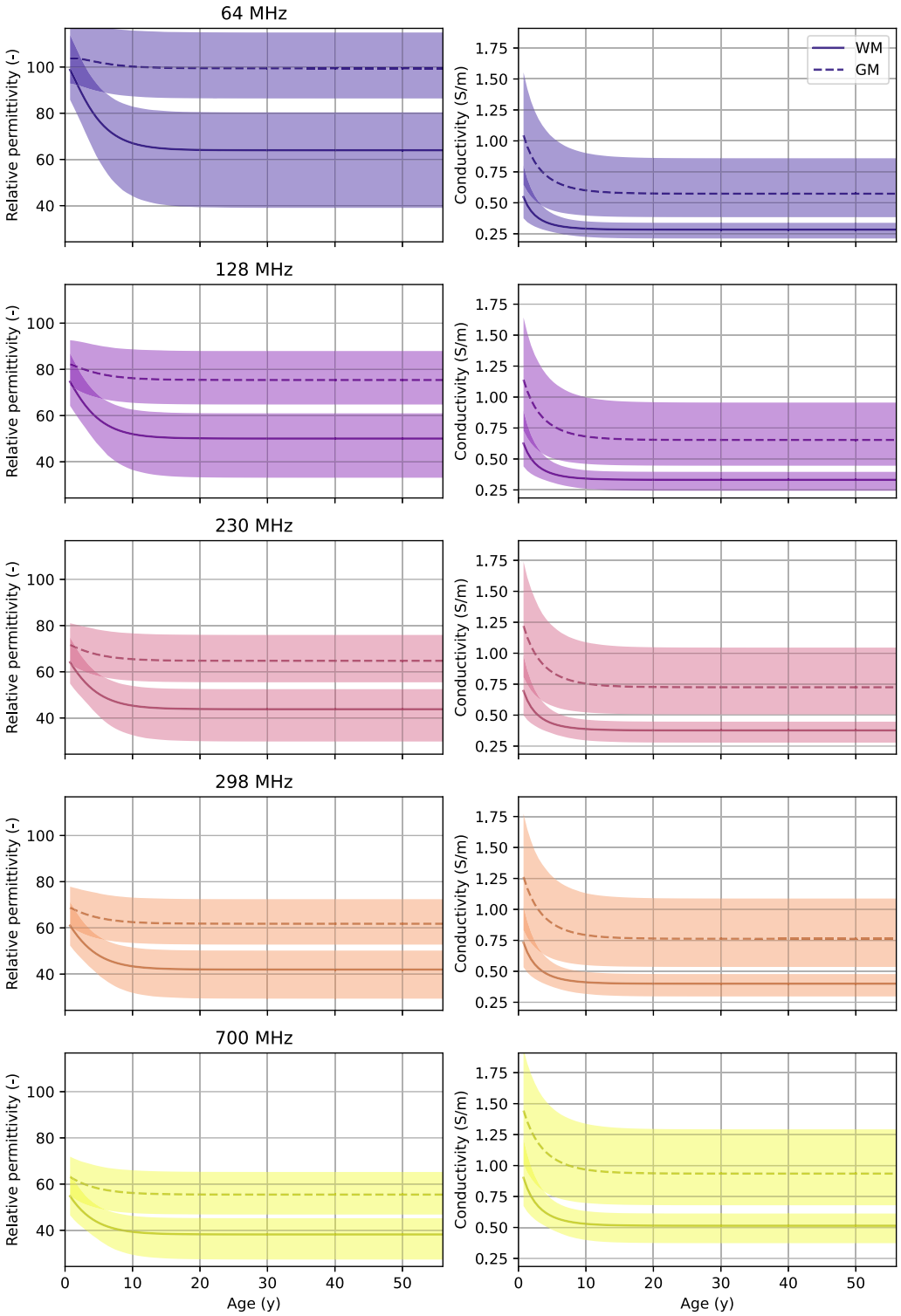

Fig. 6. Trends of relative permittivity and electrical conductivity in WM and GM at different frequencies (including 64, 128 and 298 MHz, corresponding to the proton Larmor frequencies at 1.5, 3 and 7 T respectively), as a function of age. The bands represent the corresponding 95% prediction interval.

through our model (Eqs. (2) and (3)) for a comprehensive uncertainty calculation of the curves in Fig. 5. Moreover, it is known that the choice of the T_1 mapping method can significantly impact T_1 values (see e.g. Assländer and Flassbeck (2025)), potentially affecting the results of wEPT computation. We accounted this bias by recalibrating the whole model (1) using study-specific values for T_1 (see also e.g. Mandija et al. (2018)). An additional limitation is that wEPT, by definition, derives electrical properties only from estimates of water content. While water content is an important factor for dielectric behaviour, other factors are not captured here (e.g., the concentration of free ions). Some changes over the course of normal development can modify σ and ε_r independently of the water content, possibly yielding biased EP estimates in specific situations. For this reason, the quantitative normative ranges presented here are not a substitute for direct or model-based EPT measurements when the tissue state may differ from the healthy reference. Future work should therefore aim at extension

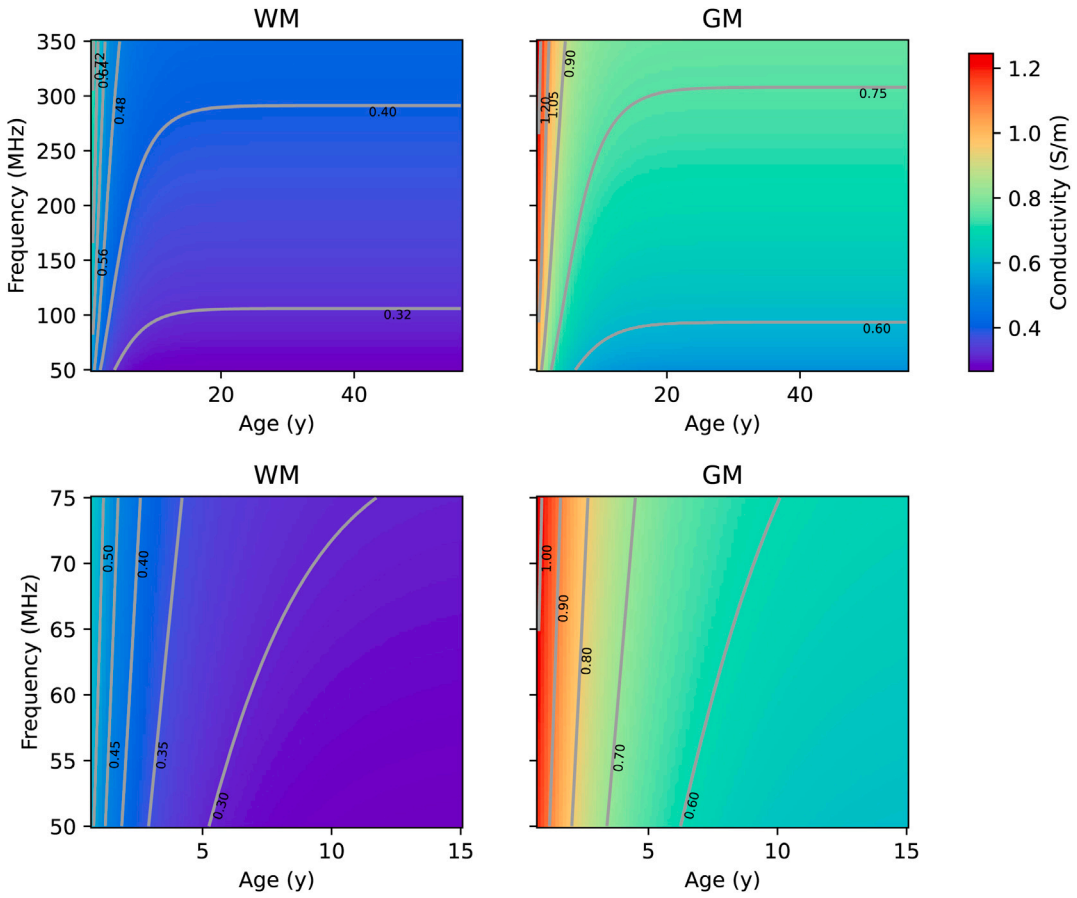

Fig. 7. Conductivity calculated according to age and frequency in the white matter (left) and grey matter (right). The second row is a zoom-in for age below 15 and frequency between 50 MHz and 75 MHz.

and validation of the present model. Finally, the applicability of the proposed method is limited to frequencies that are high enough (more than about 50 MHz) to make the electrical property values depend on the tissue composition (and, consequently, the water content) more than on the tissue structure. Indeed for WM, GM and CSF the IT'IS Foundation database uses the measurements collected in Gabriel et al. (1996b). Regarding these measurement results, the authors noted that their model is most reliable above 1 MHz and reported an increased dispersion of sample values below 100 MHz. The 50 MHz lower bound here used therefore represents also a conservative choice in terms of uncertainty in the calibration electrical property values.

On the experimental side, the work was developed based on a relatively small number of subjects. This might have produced some misestimation (under- or overestimation) of the uncertainty, even if, on the whole, data in Fig. 4 exhibit a good level of consistency. It should also be considered that the uncertainty investigated in this work is entirely deduced starting from the empirically observed intra-subject and inter-subject variability. No other contribution of measurement uncertainty (e.g., stability of the measurement system) were considered. Nevertheless, the MRF T_1 mapping approach adopted here has demonstrated high repeatability and reproducibility in a prior work (Buonincontri et al., 2021).

It is worth noticing that the model used in this work to describe the effect of age is mostly driven by the evolution of water content and dielectric properties during the developmental age. Other publications have shown that the evolution of such parameters continues during ageing for the entire lifespan, e.g., leading to an increase of T_1 values in certain brain regions from 55 to 95 years of age (Ndengera et al., 2022). Recently, similar investigations have been conducted also with reference to the electrical conductivity of brain tissues (He et al., 2024; Cao et al., 2025). In these works the conductivity has been evaluated in vivo from EPT results based on transceive phase acquisitions, rather than wEPT as for the present work. However, there is not an agreement about the actual trend of the conductivity value, that could be increasing (He et al., 2024) or decreasing (Cao et al., 2025) during ageing. Despite our work focuses on developmental age and assumes an asymptotic constant value of the properties, the 95% coverage intervals reported after 20 years of age could conceal the ageing trend, that should be further investigated in future works.

5. Conclusion

This study establishes an age-specific dielectric dispersion model for human brain tissues by integrating water content-based electrical property tomography with developmental trajectories. Linking T_1 values to dielectric properties via water content, which shows an exponential decay with age, our framework allowed age-specific conductivity and permittivity values to be derived from 50 MHz to 700 MHz (and possibly beyond). In terms of uncertainty quantification, prediction intervals incorporating intra-subject spatial heterogeneity and inter-subject variability were obtained. These contributions enable age-specific electromagnetic simulations for pediatric brain imaging and exposure safety assessments, while providing normative references for dielectric biomarkers in developing brains. Future work will focus on identifying EP ranges for pathologies, in order to assess the potential and the accuracy of EPT as a diagnostic tool. As a result of this work, we provide an open source software freely available online[1] to compute

[1] https://github.com/SebastienMarmin/brain-water-content-ept-values

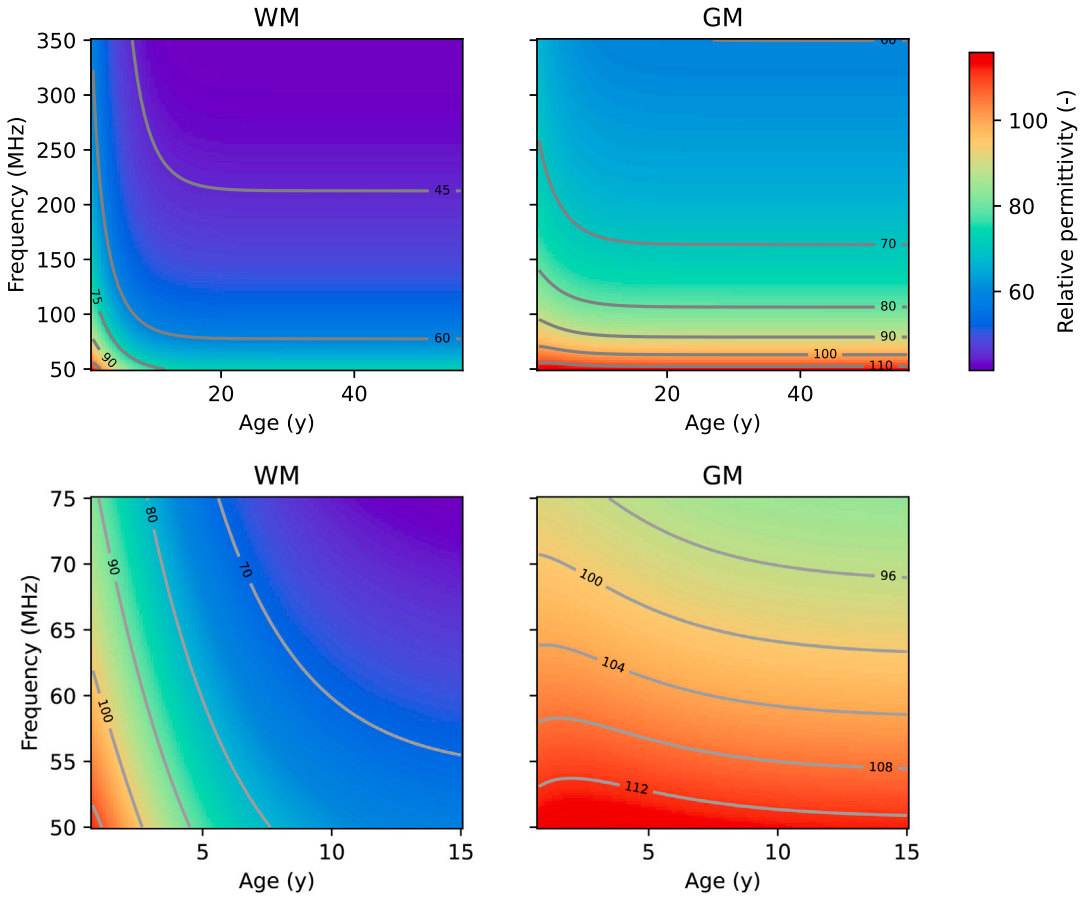

Fig. 8. Relative permittivity calculated according to age and frequency in the white matter (left) and grey matter (right). The second row is a zoom-in for age below 15 and frequency between 50 MHz and 75 MHz.

electrical properties and their uncertainties as a function of frequency and age, filling a gap in existing databases.

CRediT authorship contribution statement

Sébastien Marmin: Writing – review & editing, Writing – original draft, Visualization, Software, Project administration, Investigation, Data curation. **Alessandro Arduino:** Writing – review & editing, Writing – original draft, Validation, Software, Methodology, Investigation. **Matteo Cencini:** Writing – review & editing, Methodology, Investigation, Data curation, Conceptualization. **Marta Lancione:** Writing – review & editing, Writing – original draft, Visualization, Validation, Resources, Methodology, Investigation, Data curation. **Laura Biagi:** Writing – review & editing, Funding acquisition. **Michela Tosetti:** Writing – review & editing, Funding acquisition. **Luca Zilberti:** Writing – review & editing, Writing – original draft, Visualization, Validation, Supervision, Methodology, Investigation, Conceptualization, Funding acquisition.

Declaration of competing interest

We hereby declare that we have no financial or personal relationships with other people or organizations that could inappropriately influence or bias the work reported in this paper.

Acknowledgements

The results presented here have been developed in the framework of the 18HLT05 QUIERO and 24DIT01 APULEIO Projects. The 18HLT05 QUIERO project has received funding from the EMPIR Programme, Germany co-financed by the Participating States and from the European Union's Horizon 2020 Research and Innovation Programme. The project 24DIT01 APULEIO has received funding from the European Partnership on Metrology, co-financed from the European Union's Horizon Europe Research and Innovation Programme and by the Participating States. This study was also partially supported by the Italian Ministry of Health via the "RC 2025" to IRCCS Fondazione Stella Maris.

Data availability

Aggregated tissue water content data (median and interquartile ranges of white and grey matter water content) for all participants (including age and gender) are publicly available.

Python implementation for electrical property computation with uncertainty quantification, along with figure reproduction scripts, are publically available at https://github.com/SebastienMarmin/brain-water-content-ept-values.

References

Assländer, J., Flassbeck, S., 2025. Magnetization transfer explains most of the T1 variability in the MRI literature. Magn. Reson. Med. 94 (1), 293–301.

Baumgartner, C., Hasgall, P., Di Gennaro, F., Neufeld, E., Lloyd, B., Gosselin, M., Payne, D., Klingenböck, A., Kuster, N., 2025. IT'IS database for thermal and electromagnetic parameters of biological tissues. Online.

Bottauscio, O., Zanovello, U., Arduino, A., Zilberti, L., 2024. Polynomial chaos expansion of SAR and temperature increase variability in 3 T MRI due to stochastic input data. Phys. Med. Biol. 69 (12), 125005.

Buonincontri, G., Kurzawski, J.W., Kaggie, J.D., Matys, T., Gallagher, F.A., Cencini, M., Donatelli, G., Cecchi, P., Cosottini, M., Martini, N., Frijia, F., Montanaro, D., Gómez, P.A., Schulte, R.F., Retico, A., Tosetti, M., 2021. Three dimensional MRF

obtains highly repeatable and reproducible multi-parametric estimations in the healthy human brain at 1.5T and 3T. NeuroImage 226, 117573.
Cao, J., Philby, J., Ball, I.K., Rae1, C.D., 2025. Brain tissue conductivity decreases with age. In: Proc. Intl. Soc. Mag. Reson. Med.. p. 1508.
Cencini, M., Lancione, M., Pasquariello, R., Peretti, L., Pirkl, C.M., Schulte, R.F., Buonincontri, G., Arduino, A., Zilberti, L., Biagi, L., et al., 2024. Fast high-resolution electric properties tomography using three-dimensional quantitative transient-state imaging-based water fraction estimation. NMR Biomed. 37 (1), e5039.
Chiaramello, E., Parazzini, M., Fiocchi, S., Ravazzani, P., Wiart, J., 2018. Stochastic dosimetry based on low rank tensor approximations for the assessment of children exposure to WLAN source. IEEE J. Electromagn. RF Microw. Med. Biol. 2 (2), 131–137.
Cho, S., Jones, D., Reddick, W.E., Ogg, R.J., Steen, R., 1997. Establishing norms for age-related changes in proton T1 of human brain tissue in vivo. Magn. Reson. Imaging 15 (10), 1133–1143.
Fatouros, P.P., Marmarou, A., 1999. Use of magnetic resonance imaging for in vivo measurements of water content in human brain: method and normal values. J. Neurosurg. 90 (1), 109–115.
Fiocchi, S., Markakis, I.A., Ravazzani, P., Samaras, T., 2013. SAR exposure from UHF RFID reader in adult, child, pregnant woman, and fetus anatomical models. Bioelectromagnetics 34, 443–452.
Gabriel, C., Gabriel, S., Corthout, Y., 1996a. The dielectric properties of biological tissues: I. Literature survey. Phys. Med. Biol. 41 (11), 2231.
Gabriel, S., Lau, R., Gabriel, C., 1996b. The dielectric properties of biological tissues: II. Measurements in the frequency range 10 Hz to 20 GHz. Phys. Med. Biol. 41 (11), 2251.
Gabriel, S., Lau, R., Gabriel, C., 1996c. The dielectric properties of biological tissues: III. Parametric models for the dielectric spectrum of tissues. Phys. Med. Biol. 41 (11), 2271.
Gabriel, C., Peyman, A., 2018. Dielectric properties of biological tissues; variation with age. Conn's Handb. Model. Hum. Aging 939–952.
Gilbert, K.M., Nichols, E.S., Gati, J.S., Duerden, E.G., 2023. A radiofrequency coil for infants and toddlers. NMR Biomed. 36 (8), e4928.
Gómez, P.A., Cencini, M., Golbabaee, M., Schulte, R.F., Pirkl, C., Horvath, I., Fallo, G., Peretti, L., Tosetti, M., Menze, B.H., et al., 2020. Rapid three-dimensional multiparametric MRI with quantitative transient-state imaging. Sci. Rep. 10 (1), 13769.
Gräfe, D., Frahm, J., Merkenschlager, A., Voit, D., Hirsch, F.W., 2021. Quantitative T1 mapping of the normal brain from early infancy to adulthood. Pediatr. Radiol. 51, 450–456.
He, Z., Soullié, P., Lefebvre, P., Ambarki, K., Felblinger, J., Odille, F., 2024. Changes of in vivo electrical conductivity in the brain and torso related to age, fat fraction and sex using MRI. Sci. Rep. 14, 16109.
Isensee, F., Schell, M., Pflueger, I., Brugnara, G., Bonekamp, D., Neuberger, U., Wick, A., Schlemmer, H.-P., Heiland, S., Wick, W., Bendszus, M., Maier-Hein, K.H., Kickingereder, P., 2019. Automated brain extraction of multisequence MRI using artificial neural networks. Hum. Brain Mapp. 40 (17), 4952–4964.
Joint committee for guides in metrology (JCGM), 2008a. Evaluation of Measurement Data—Guide to the Expression of Uncertainty in Measurement. BIPM, Paris, France.
Joint committee for guides in metrology (JCGM), 2008b. Supplement 1 to the "Guide to the Expression of Uncertainty in Measurement" - Propagation of Distributions using a Monte Carlo Method. BIPM, Paris, France.
Lancione, M., Cencini, M., Scaffei, E., Cipriano, E., Buonincontri, G., Schulte, R.F., Pirkl, C.M., Buchignani, B., Pasquariello, R., Canapicchi, R., et al., 2024. Magnetic resonance fingerprinting-based myelin water fraction mapping for the assessment of white matter maturation and integrity in typical development and leukodystrophies. NMR Biomed. 37 (6), e5114.
Lesbats, C., Katoch, N., Minhas, A.S., Taylor, A., Kim, H.J., Woo, E.J., Poptani, H., 2021. High-frequency electrical properties tomography at 9.4 T as a novel contrast mechanism for brain tumors. Magn. Reson. Med. 86 (1), 382–392.
Liu, J., Wang, Y., Katscher, U., He, B., 2017. Electrical properties tomography based on B_1 maps in MRI: Principles, applications, and challenges. IEEE Trans. Biomed. Eng. 64 (11), 2515–2530.
Malik, S.J., Hand, J.W., Carmichael, D.W., Hajnal, J.V., 2022. Evaluation of specific absorption rate and heating in children exposed to a 7T MRI head coil. Magn. Reson. Med. 88 (3), 1434–1449.
Malik, S.J., Hand, J.W., Satnarine, R., Price, A.N., Hajnal, J.V., 2021. Specific absorption rate and temperature in neonate models resulting from exposure to a 7T head coil. Magn. Reson. Med. 86 (3), 1299–1313.
Mandija, S., Jacobs, S.M., Kleinloog, J.P., Liu, H., van der Heide, O., Kolk, A.G., Sbrizzi, A., van den Berg, C.A., 2023. Water content-based electrical properties tomography: results from a retrospective clinical study. http://dx.doi.org/10.21203/rs.3.rs-2826996/v1.
Mandija, S., Petrov, P.I., Vink, J., Neggers, S.F., Luijten, P.R., van den Berg, C.A., 2018. In-vivo validation of water content electrical properties tomography reconstructions in white matter using independent MR-EPT measurements. In: Proc 26th Sci Meet Int Soc Mag Reson Med Paris (FR). Vol. 5096.
McGivney, D.F., Pierre, E., Ma, D., Jiang, Y., Saybasili, H., Gulani, V., Griswold, M.A., 2014. SVD compression for magnetic resonance fingerprinting in the time domain. IEEE Trans. Med. Imaging 33 (12), 2311–2322.
Michel, E., Hernandez, D., Lee, S.Y., 2017. Electrical conductivity and permittivity maps of brain tissues derived from water content based on T1-weighted acquisition. Magn. Reson. Med. 77 (3), 1094–1103.
Ndengera, M., Delattre, B.M.A., Scheffler, M., Lövblad, K.-O., Meling, T.R., Vargas, M.I., 2022. Relaxation time of brain tissue in the elderly assessed by synthetic MRI. Brain Behav. 12 (1), e2449.
Park, J.A., Kang, K.J., Ko, I.O., Lee, K.C., Choi, B.K., Katoch, N., Kim, J.W., Kim, H.J., Kwon, O.I., Woo, E.J., 2019. In vivo measurement of brain tissue response after irradiation: Comparison of T2 relaxation, apparent diffusion coefficient, and electrical conductivity. IEEE Trans. Med. Imaging 38 (12), 2779–2784.
Peyman, A., Gabriel, C., Grant, E., Vermeeren, G., Martens, L., 2009. Variation of the dielectric properties of tissues with age: The effect on the values of SAR in children when exposed to walkie–talkie devices. Phys. Med. Biol. 54 (2), 227.
Peyman, A., Holden, S., Watts, S., Perrott, R., Gabriel, C., 2007. Dielectric properties of porcine cerebrospinal tissues at microwave frequencies: in vivo, in vitro and systematic variation with age. Phys. Med. Biol. 52 (8), 2229.
Peyman, A., Rezazadeh, A., Gabriel, C., 2001. Changes in the dielectric properties of rat tissue as a function of age atmicrowave frequencies. Phys. Med. Biol. 46 (6), 1617.
Romascano, D., Piredda, G.F., Caneschi, S., Hilbert, T., Corredor, R., Maréchal, B., Kober, T., Ledoux, J.-B., Fornari, E., Hagmann, P., et al., 2024. Normative volumes and relaxation times at 3T during brain development. Sci. Data 11 (1), 429.
Thurai, M., Goodridge, V., Sheppard, R., Grant, E., 1984. Variation with age of the dielectric properties of mouse brain cerebrum. Phys. Med. Biol. 29 (9), 1133.
Thurai, M., Steel, M., Sheppard, R., Grant, E., 1985. Dielectric properties of developing rabbit brain at 37 C. Bioelectromagn.: J. Bioelectromagn. Soc. Soc. Phys. Regul. Biol. Med. Eur. Bioelectromagn. Assoc. 6 (3), 235–242.
Uecker, M., Lai, P., Murphy, M.J., Virtue, P., Elad, M., Pauly, J.M., Vasanawala, S.S., Lustig, M., 2014. ESPIRiT—an eigenvalue approach to autocalibrating parallel MRI: Where SENSE meets GRAPPA. Magn. Reson. Med. 71 (3), 990–1001.
Wang, J., Fujiwara, O., Watanabe, S., 2006. Approximation of aging effect on dielectric tissue properties for SAR assessment of mobile telephones. IEEE Trans. Electromagn. Compat. 48 (2), 408–413.
Weigel, M., 2015. Extended phase graphs: Dephasing, RF pulses, and echoes - pure and simple. J. Magn. Reson. Imaging 41 (2), 266–295.
Zhang, Y., Brady, M., Smith, S., 2001. Segmentation of brain MR images through a hidden Markov random field model and the expectation-maximization algorithm. IEEE Trans. Med. Imaging 20 (1), 45–57.
Zhang, X., Liu, J., He, B., 2014. Magnetic-Resonance-based electrical properties tomography: A review. IEEE Rev. Biomed. Eng. 7, 87–96.